

1 **Flow-Substrate Interactions in Aggrading and Degrading Submarine Channels**

2 **Anjali M. Fernandes^{1,2}, James Buttles¹, David Mohrig¹, Kyle M. Straub³**

3 *¹The Center for Integrative Geoscience, University of Connecticut, Storrs, Connecticut, USA.*

4 *²The Jackson School of Geosciences, The University of Texas at Austin, Texas, USA.*

5 *³Department of Earth and Environmental Sciences, Tulane University, 6823 St. Charles Avenue, New*
6 *Orleans, Louisiana 70118-5698, USA*

7 *Email: anjali.fernandes@uconn.edu*

8 Keywords: Turbidity currents; submarine channels; submarine canyons; boundary layer roughness; flow-
9 separation zones; erosional bedforms; detachment-limited channels; transport-limited channels; Shields
10 scaling

11 **ABSTRACT**

12 Connecting real time measurements of current-bed interactions to the temporal evolution of
13 submarine channels can be extremely challenging in natural settings. We present a suite of physical
14 experiments that offer insight into the spectrum of interactions between turbidity currents and their
15 channels, from (i) detachment-limited erosion to (ii) transport-limited erosion to (iii) pure deposition. In
16 all three cases channel sinuosity influenced patterns of erosion and deposition; the outsides of bends
17 displayed the highest erosion rates in the first two cases, whereas the outsides of bends were associated
18 with the highest deposition rates the third. We connect the evolution of these channels to the turbulence of
19 the near-bed boundary layer. In the erosional experiments both channel beds roughened through time,
20 developing erosional bedforms or trains of ripples. Reynolds estimates of boundary layer roughness
21 indicate that, in both erosional cases, the near-bed boundary layer roughened from smooth or
22 transitionally rough to rough, whereas the depositional channel appears to have remained consistently
23 smooth. Our results suggest that, in the absence of any changes from upstream, erosion in submarine

24 channels erosion is a self-reinforcing mechanism whereby developing bed roughness increases turbulence
25 at the boundary layer, thereby inhibiting deposition, promoting sediment entrainment and enhancing
26 channel relief; deposition occurs in submarine channels when the boundary layer remains smooth,
27 promoting aggradation and loss of channel relief.

28 **INTRODUCTION**

29 Continental margins are patterned with channels and canyons that convey large volumes of
30 sediment to the deep ocean. These channels evolve through erosion and/or deposition, often aggrading
31 over significant vertical distances (Pirmez et al., 2000), or by carving canyons (Babonneau et al., 2010;
32 Conway et al., 2012) many hundreds of meters deep. Physical experiments can offer insight into current-
33 bed interactions. Such measurements are challenging to acquire in natural settings and even more
34 challenging to relate to the temporal evolution of submarine channels (Khripounoff et al., 2003; Xu et al.,
35 2004, 2013; Xu, 2010; Hughes Clarke, 2016; Symons et al., 2017; Azpiroz-Zabala et al., 2017b, 2017a).
36 In the past, some experiments e.g. (Mohrig and Buttle, 2007; Straub et al., 2008; Janocko et al., 2013)
37 focused on purely depositional turbidity currents that were suspension-dominated, whereas others
38 investigated erosional currents that modified channels primarily through bedload-transport (Métivier et
39 al., 2005; Amos et al., 2010). Here we present three experiments which we use to explore the processes
40 that shape submarine channels, along the continuum of intensely erosional to purely depositional in
41 connection to the hydraulic characteristics of the near-bed boundary layer, across this spectrum of
42 behaviour.

43 **Detachment-limited and transport-limited erosion in terrestrial landscapes**

44 Terrestrial channels eroding into bedrock have been modeled using: a) a detachment-limited model
45 in which the resistance of the substrate is the limiting factor that controls the erosion rate, and b) a transport-
46 limited model where the erosion rate is limited by the ability to transport the eroded sediment (Howard,
47 1980, 1994; Whipple, 2004). Detachment-limited erosion is more sensitive to local conditions (e.g.
48 topographic or bed roughness) rather than reach-averaged conditions (e.g. discharge; (Johnson and

49 Whipple, 2007). Erosion generally takes place through abrasion and wear by the impacts of sediment being
50 transported by the flow, and turbulence generated by evolving bed roughness. These channels are
51 characterized by knickpoints, inner channels, scour holes, grooves, and sculpted bedforms (Whipple, 2004).
52 The transporting currents are efficient at removing sediment in transport from upstream and at entraining
53 material from the local substrate.

54 When the removal of eroded sediment is not efficient, sediment is stored in patches on the bed,
55 protecting the bed from further erosion in a phenomenon referred to as the ‘cover-effect’ (Johnson et al.,
56 2009). Erosional channels with abundant sediment cover on the channel bed are referred to as “transport-
57 limited” (Shepherd and Schumm, 1974; Sklar and Dietrich, 2004; Whipple, 2004; Johnson and Whipple,
58 2007). Partially-alluviated erosional channels scouring into compact, indurated sediment have been
59 observed in depositional landscapes such as the Mississippi River Delta (Edmonds et al., 2011; Nittrouer
60 et al., 2011a), where cover effects are particularly evident. Channel bottoms display deep scours where they
61 are devoid of alluvial cover at the outsides of river bends. All natural erosional channels can be expected to
62 display some combination of detachment-limited and transport-limited behaviour (Whipple, 2004). Here
63 we use 2 experiments to study the characteristics of detachment-limited and transport-limited erosion in
64 submarine channels. For completeness, we incorporate data from an aggradational channel experiment
65 (Straub et al., 2008). We use these experiments to explore the role of the near-bed boundary layer in the
66 spectrum of forms and deposit characteristics observed.

67 **Dynamic scaling of experiments to natural systems**

68 Laboratory experiments have historically been compared to natural systems by using three
69 dimensionless variables: (1) the densimetric Froude number (Fr_d), (2) the Reynolds number (Re), and (3)
70 the ratio of current shear velocity u^* to particle fall velocity w_s (Middleton, 1966; Baas et al., 2004; Yu et
71 al., 2006; Mohrig and Buttle, 2007; Straub et al., 2008; Amos et al., 2010; Rowland et al., 2010; Cantelli
72 et al., 2011). The first parameter, the Froude number, defines the ratio between momentum and
73 gravitational forces within the transporting current and is traditionally maintained equal or similar to

74 natural analogues. The Reynolds number, which quantifies the turbulence of the currents, cannot be equal
75 to natural flows in scaled-down laboratory settings. The third parameter, also referred to as a Shield's
76 parameter (Shields, 1936; Bagnold, 1966; Smith and Hopkins, 1971; van Rijn Leo C., 1984; Nino et al.,
77 2003), characterizes how sediment is transported. Flows in which the turbulent shear, expressed as the
78 shear velocity u^* , is significantly larger than the gravitational settling velocity w_s will be more competent
79 at transporting sediment in suspension over significant distances (Shields, 1936; Smith and Hopkins,
80 1971) and will prelude sediment-bed interactions over short length scales; if u^* is comparable to w_s ,
81 sediment can be transported as either saltating or incipiently suspended load, dependent upon the intensity
82 of turbulence associated with current-bed interactions. In channelized turbidity currents, the intensity of
83 near-bed turbulence is the combined result of turbulent eddies shed at the scale of individual particles (de
84 Leeuw et al., 2016), of bed roughness (e.g. bedforms, scours, etc.) (Eggenhuisen et al., 2010;
85 Eggenhuisen and McCaffrey, 2012; Arfaie et al., 2018), as well as of planform irregularities (e.g. curved
86 channels) (Straub et al., 2011) which can impart turbulent shear from non-uniform spatial accelerations.
87 The magnitude of turbulence will scale with the magnitudes of fluid shear (u^*) and the size of the element
88 under consideration (e.g. particle diameter, dune height, scour depth, bend amplitude, etc.). Turbulence
89 associated with these roughness scales contributes to entrainment of sediment from the bed and walls of
90 channels, and encourages vertical mixing which maintains sediment in suspension. The ratio between
91 fluid shear and the viscous forces which act to damp turbulence can be used to characterize the roughness
92 of the near-bed boundary layer (Garcia, 2008).

93 De Leeuw et al. (2016) argued that realistic turbulence-sediment interactions were critical for
94 effectively modelling submarine channel inception and evolution, and proposed a scaling approach defined
95 by the ratio of the Shield's parameter to the particle Reynolds number (Re_p). In this scaling approach, the
96 Shield's parameter is held similar between experimental and naturally occurring density currents, but the
97 similarity between the particle Reynolds numbers is relaxed as long as the boundary layer is rough or
98 transitionally rough (Garcia, 2008; de Leeuw et al., 2016). Leeuw et al. (2017) noted that density currents

99 in most previous experiments were highly depositional because the boundary layers were hydraulically
100 smooth and/or the Shields parameter fell below the initiation of suspension.

101 In Figure 1, we adopt the Shield's scaling proposed by de Leeuw et al. (2016) to compare flow and
102 sediment transport characteristics of the three experiments presented here to past experimental and field
103 measurements. Although the shear stresses associated with all three experiments exceeded the threshold for
104 the initiation of suspension, they straddle the threshold between hydraulically smooth and transitionally
105 rough boundary layers. Furthermore, Experiments 1 and 2 scale best with recent field observations of flow
106 and transport in natural systems. Using sediment with much lower densities than silica in these experiments
107 allowed us to use sand-sized particles that had transitionally rough boundary layers and high Shields
108 parameters, and were therefore easy to suspend and maintain in suspension.

109 **Experiment Design**

110 In each experiment, calcium chloride salt and water (and sediment, when it was used), were mixed
111 together in a reservoir, until the salt was completely dissolved. The mixture was agitated over several hours
112 and allowed to cool to room temperature, as the dissolution of this salt in water is an exothermic process.
113 Once at room temperature, the mixture was pumped up to a constant head tank and then allowed to flow
114 into the experimental basin at a controlled rate set by the constant hydraulic head and a system of valves.
115 The two experimental basins were designed along similar lines, shown by the generalized schematic in
116 Figure 2. In all experiments, density currents were released into an experimental channel through a box
117 with two perforated screens designed to extract momentum from flows. The pre-formed channels were built
118 upon a platform separated from the walls of the basin by deep moats that prevented currents from reflecting
119 off the basin walls. Saline fluid was not allowed to collect in the basin and was extracted through the floor
120 drains as it flowed off the raised platform. The water level in the basin was maintained with a constant flux
121 of fresh water and overflow drainage through a weir. The basin used in Experiment 1 was 8 m long, 6 m
122 wide and 2 m deep. The basin used for Experiments 2 & 3 was 5 m long, 4.5 m wide and 0.8 m deep. In all
123 experiments, the channel was constructed diagonally across the false floor.

124 The channels used in these experiments were designed with similar sinuosity, but different
 125 sediment and flow properties (Table 1). In Experiment 1, the channel was built entirely out of a weakly
 126 cohesive mixture of acrylic particles (specific gravity = 1.15) and clay positioned on top of a sloping ramp.
 127 The sediment was mixed in a 10:1 volumetric ratio. The first two currents released into the channel were
 128 saline density currents (excess density = 4%). These were followed by three more density currents that
 129 carried a 2% volumetric concentration of suspended acrylic sediment.

130 In Experiment 2 a saline density current (excess density = 3.32%) was released through the
 131 experimental channel which consisted of a cohesionless, 2-cm thick bed of acrylic particles draped over a
 132 sinuous channel form built from concrete. In Experiment 3 sixteen purely depositional currents flowed
 133 through a channel constructed of concrete with a thin layer of silica sediment on the bed. Currents had an
 134 excess density of 2.1%. 33% of this excess density was supplied by suspended sediment in the current, and
 135 the remaining 67% was from dissolved salt. High-resolution bathymetry maps (horizontal resolution =
 136 4mm; vertical resolution ~100 microns for Experiments 1 & 2; ~1mm for Experiment 3), collected before
 137 and after each flow defined patterns of bed change for all three cases. Key geometric and dynamic properties
 138 of the experimental designs are compiled in Table 1.

139 **Table 1: Summary of geometric and dynamic properties of Experiments 1, 2 and 3.**

	Parameter	Experiment 1	Experiment 2	Experiment 3
Channel geometry	Channel depth (m)	0.15	0.09	0.11
	Channel width (m)	0.50	0.40	0.40
	Down-channel slopes (degrees)	7.00	2.00	1.00
	Initial mean thickness of erodible bed (m)	0.07	0.02	0.00
	Channel sinuosity	1.15	1.28	1.28
Sediment properties	Sediment density (ρ_s) (kg/m ³)	1150.00	1150.00	2650.00
	D ₁	49	49	1.7
	D ₁₀	88	88	12.9
	D ₂₅	127	127	23
	D ₅₀	146	146	31
	D ₇₅	205	205	41
	D ₉₀	243	243	52.1
	D ₉₉	340	340	80
Flow properties	Flow thickness (m)	0.10	0.09	0.10
	Current density (ρ_f) (kg/m ³)	1040	1033.20	1021
	Depth-averaged downstream velocity (u) (m/s)	0.10	0.05	0.08
	Shear velocity (u*) (m/s)	0.04	0.03	0.04
	Froude number (Fr)	0.50	0.26	0.56
	Reynolds number (Re)	10000.00	4050.00	8000.00

	Particle Reynolds number (Re_p)	6.53	4.38	1.24
	Shields parameter	13.20	5.56	3.30
	Bed roughness scale (H_{bed}) (m)	0.01 - 0.05	0.01 - 0.02	-
	Reynolds number from bed roughness (Re_{bed})	~650 - 2236	~330- 660	-

140

141 **Results**

142 Integrating surface change for each flow in all three cases reveal net erosion in Experiments 1 and
143 2, and net deposition in Experiment 3.

144 **Experiment 1**

145 In Experiment 1, all 5 currents released through the channel modified it through net erosion (Fig.
146 3 A, Fig. 4). The weakly cohesive bed consisted of sediment that was easily suspended once it detached
147 from the surface (Fig. 1). Extreme run-up of currents onto the outer walls of channel bends occurred,
148 resulting in the formation of a low-velocity flow-separation zone (depth-averaged velocity \sim 1-2 m/s) at
149 the inner bank (Fig. 4G; Fig.5) (Leeder and Bridges, 1975; Fernandes et al., 2018). Erosion occurred
150 beneath the pathway of the high-velocity (depth-averaged velocity = 10m/s) core of the current, which
151 travelled along the outside of bends and created a series of discontinuous scours. Initially, while the channel
152 bed was smooth, the most intense scouring occurred at the outside of bends (Fig. 4A, B, H; Fig. 6).
153 Subsequently, the rough edges of scours became sites of focussed erosion (Fig. 4C-F, I-L; Fig. 6A-C) and
154 resultant elongation of scours resulted in the formation of a discontinuous inner channel (Fig. 7A- B).
155 Focussed erosion at the downstream edges of scours released clouds of suspended sediment that were
156 transported downstream and out of the system. Consecutive inner bank areas were separated by a swath of
157 erosion, and evolved into raised terraces within the low-velocity flow separation zone (Fig. 3A, Fig. 4;
158 (Fernandes et al., 2018). The channel bed evolved from smooth to ornamented, displaying erosional
159 bedforms with centimeter-scale relief (Fig. 3A; Fig. 6). These bed morphologies are similar to those
160 observed in detachment-limited terrestrial channels, where erosion is limited by the strength of the substrate
161 and bed erosion occurs primarily through wear by abrasion and plucking (Whipple et al., 2000; Whipple,
162 2004). The channel remained net-erosional through its entire length (Fig. 3A; Fig. 4).

163 **Experiment 2**

164 This channel was modified through net-erosion, with a fraction of mobilized sediment leaving the
165 system in suspension while the remainder was reworked into a continuous train of bedforms (Fig. 3B). As
166 in Experiment 1, the high velocity core of the density current travelled along the outsides of bends, resulting
167 in: 1) erosion of sediment at the outer bank, where sediment removal exposed the underlying erosion-
168 resistant channel form in the troughs between sediment-starved bedforms, and 2) deposition at the inner
169 bank, which resulted from the convergence of downstream and cross-stream bedload transport (Fig. 3B,
170 Fig 7C-D). These zones of deposition began just upstream from the points of maximum channel curvature,
171 and were connected across inflection points through the continuous bedform field (Fig. 4B). Erosion in this
172 experiment was less efficient than in Experiment 1. Abundant sediment cover on the channel bed is
173 suggestive of erosional mechanics similar to that of transport-limited erosional terrestrial channels, which
174 are also characterized by alluviated channel beds interrupted by variable degrees of local scouring
175 (Whipple, 2004; Nittrouer et al., 2011a, 2011b), and in which the erosion rate is limited by the ability of
176 the flow to transport the eroded sediment.

177 **Experiment 3**

178 Currents modified this channel via net sediment deposition (Straub et al., 2008). The thickest
179 deposition closely tracked the pathway of the high velocity core, which was inferred to be the pathway of
180 the highest suspended sediment concentration (Fig. 9 of Straub et al., 2008). This resulted in thicker deposits
181 at the outer banks of bends and thinner deposits in low-velocity zones at the inner banks of bends (Fig. 3C,
182 Fig. 7E-F). Deposits from each current draped the entire channel (Fig. 7E-F), and thinned in the downstream
183 direction (Fig. 6D-F). Sediment was primarily transported as and deposited from suspended load.
184 Suspended sediment flux was estimated to be roughly 40 times that of bedload flux (Straub et al., 2008).

185 **Discussion**

186 **Boundary layer roughness in erosional and depositional channels**

187 The transporting currents in all three experiments had shear stresses that were high enough to
188 transport sediment in suspension. Yet their temporal evolution spanned the spectrum from intense erosion
189 to pure deposition. In all three cases, planform irregularity influenced the spatial variability in sedimentation
190 and/or erosion by influencing the path of the highest velocities and sediment concentrations. A key
191 difference between the 3 experiments lies in the characteristics of the hydraulic boundary layer and the
192 temporal evolution of the three channels suggests strong agreement with the Shield-scaling predictions of
193 de Leeuw et al., 2016. Particle-scale Reynolds estimates of boundary layer turbulence place Experiment 1
194 in the transitionally rough hydraulic regime, whereas Experiment 2 was at the approximate boundary
195 between the smooth and transitionally rough regime, and Experiment 3 was squarely within the
196 hydraulically smooth regime. Furthermore, Experiment 1 evolved from a smooth bed to one patterned by
197 scours, grooves and other centimeter-scale erosional bedforms; Experiment 2 evolved from a smooth bed
198 into a semi continuous bedform field. In both erosional experiments the roughening of the channel bed is
199 likely to have encouraged greater turbulence at the near-bed boundary (Fig. 2).

200 At the start of Experiment 1, the smooth sediment bed was modified by erosion along the pathway
201 of the high velocity core; the magnitude of erosion appeared to be greatest near the outsides of bends (Fig.
202 4A, B, G, H). Particle Reynolds numbers calculated from mean, depth-averaged downstream velocities at
203 the outsides (0.1 m/s) and insides (0.01 - 0.02 m/s) of bends point to a hydraulically smooth boundary layer
204 within the flow separation zone at the inside of the bend, and a transitionally rough boundary layer at the
205 outside (Fig. 2). The emergence of erosional roughness with 1-5 centimeter relief is likely to have further
206 roughened the boundary layer, prohibiting sediment deposition and increasing erosion at sites with
207 enhanced roughness (Fig. 3A; Fig. 4; Fig.6). Near bed turbulence increased by at least two orders of
208 magnitude ($Re_{bed} \sim 450$ for 1cm relief; $Re_{bed} \sim 2200$ for 5cm relief; Fig. 2), causing a regime shift towards
209 a hydraulically rough boundary layer (Garcia, 2008). Hydraulically smooth boundary layers in flow
210 separation zones at the inner banks (Fig. 2) precluded erosion and very low suspended sediment fluxes were
211 unfavourable for deposition. Overall, Experiment 1 evolved in such a way that sediment entrainment and

212 removal remained efficient through time, and channel relief consistently increased as currents scoured into
213 the ~7cm thick erodible sediment bed (Fig. 6A; Fig 7A). Detachment-limited erosion is indicated by
214 evolution of sculpted erosional bedforms, efficient sediment removal and enhanced erosion linked to local
215 bed roughness. The temporal evolution of this channel therefore offers significant insights into the evolution
216 of topography and flow-bed interactions in detachment-limited erosional submarine channels and canyons
217 e.g. (Conway et al., 2012; Vachtman et al., 2013; Mitchell, 2014) that incise into compacted or indurated
218 fine-grained sediment on the upper continental slope and are efficient, dominantly-erosional conduits for
219 sediment transport into the deep ocean.

220 Like Experiment 1, Experiment 2 also evolved from a smooth bed to a rough one and the outer
221 banks of bends were sites of enhanced erosion. Using ripple crest height of 1-2 cm as the relevant length
222 scale, Reynolds estimates indicate that the boundary layer evolved to become hydraulically rough (Fig. 2;
223 (Garcia, 2008), though it was at the threshold between hydraulically smooth and transitionally rough at the
224 start of the experiment (Table 1). The Shields parameter for all particle sizes present falls above the
225 threshold for initiation of suspension (Shields, 1936; Bagnold, 1966; Smith and Hopkins, 1971; van Rijn
226 Leo C., 1984; Nino et al., 2003), suggesting that the rate of erosion was limited by the currents' capacity to
227 transport the sediment in suspension, and that the sediment that could not be suspended was transported as
228 bedload. The development of a bedform field, while it likely facilitated sediment entrainment by roughening
229 the boundary layer probably also reduced fluid momentum and the capacity of the current to suspend
230 sediment. This style of transport-limited erosion (Whipple, 2004; Johnson and Whipple, 2007) likely offers
231 insight into the delicate balance of flow-sediment feed-backs that control spatially variable sedimentation
232 and erosion in dominantly bypassing submarine channels on the middle or lower continental slope.

233 Unlike Experiments 1 and 2, Experiment 3 remained depositional for the duration of the
234 experiment. Straub et al., (2008) noted that super-critically climbing ripples were present over only
235 approximately 5% of the sediment bed. Consistent deposition and reduction in channel relief (Straub et al.,
236 2008) through time suggests that the boundary layer characteristics likely shifted further into the

237 hydraulically smooth regime. We suggest that this style of evolution would be most characteristic of
238 channels near the terminus of submarine transport systems, on terminal lobes on the basin flow where
239 sediment is delivered by depletive flows that are unable to re-entrain sediment.

240 **CONCLUSIONS**

241 It is extremely challenging to connect current-bed interactions to the temporal evolution of
242 submarine channels in natural settings (Khripounoff et al., 2003; Xu et al., 2004, 2013; Xu, 2010; Hughes
243 Clarke, 2016; Symons et al., 2017; Azpiroz-Zabala et al., 2017b, 2017a). We used 3 experiments in which
244 we relate near bed turbulence, as a function of evolving bed roughness, to patterns of erosion and
245 deposition. In all three experiments presented here, channel sinuosity influenced patterns of erosion and
246 deposition. Although the currents used in all three case displayed shear stresses high enough to suspended
247 sediment, the temporal evolution in the turbulence near-bed boundary layer was also very important in
248 deciding whether the channel evolved through erosion or deposition. In the experiments where the
249 boundary layer was transitionally rough the channel evolved through erosion, developing a roughened
250 bed. In both cases, the near-bed boundary layer roughened from smooth or transitionally rough to rough,
251 enhancing near-bed turbulence. When the channel substrate was cohesive, the channel bed evolved
252 through detachment-limited erosion and most of the sediment left the system in suspension. The channel
253 bed was patterned by erosional bedforms, grooves, inner-bank terraces and a semi-continuous inner
254 channels. When the sediment was non-cohesive, the erosion was limited by the ability of the currents to
255 transport sediment and the channel bed evolved into trains of ripples. In contrast, the channel with a
256 hydraulically smooth boundary layer evolved through consistent deposition and the boundary layer
257 appears to have remained hydraulically smooth. To our knowledge, this work presents the first instance in
258 which detachment-limited erosional channels with realistic sediment transport patterns and sediment-
259 turbulence interactions have been designed successfully in laboratory settings. Our results suggest that
260 erosion in submarine channels is a self-reinforcing mechanism whereby developing bed roughness
261 increases turbulence at the boundary layer, enhancing erosion and inhibiting deposition; deposition in

262 submarine channels occurs if the boundary layer is smooth, promoting channel aggradation and loss of
263 channel relief.

264 **Acknowledgements**

265 We thank the Jackson School of Geosciences, the CSM-UT RioMAR Industry Consortium, and
266 Shell International Exploration and Production Inc. for facilities and financial support of this work.

267 **References cited**

- 268 Alexander, J., McLelland, S.J., Gray, T.E., Vincent, C.E., Leeder, M.R., and Ellett, S., 2007, Laboratory
269 sustained turbidity currents form elongate ridges at channel mouths: Channel mouth deposition from
270 sustained turbidity currents: *Sedimentology*, v. 55, p. 845–868, doi:10.1111/j.1365-
271 3091.2007.00923.x.
- 272 Amos, K.J., Peakall, J., Bradbury, P.W., Roberts, M., Keevil, G., and Gupta, S., 2010, The influence of
273 bend amplitude and planform morphology on flow and sedimentation in submarine channels: *Marine*
274 *and Petroleum Geology*, v. 27, p. 1431–1447, doi:10.1016/j.marpetgeo.2010.05.004.
- 275 Arfaie, A., Burns, A.D., Dorrell, R.M., Ingham, D.B., Eggenhuisen, J.T., and McCaffrey, W.D., 2018,
276 Optimisation of flow resistance and turbulent mixing over bed forms: *Environmental Modelling &*
277 *Software*, v. 107, p. 141–147, doi:10.1016/j.envsoft.2018.06.002.
- 278 Azpiroz-Zabala, M., Cartigny, M.J.B., Sumner, E.J., Clare, M.A., Talling, P.J., Parsons, D.R., and
279 Cooper, C., 2017a, A General Model for the Helical Structure of Geophysical Flows in Channel
280 Bends: General model for helical flows in bends: *Geophysical research letters*, v. 44, p. 11,932–
281 11,941, doi:10.1002/2017GL075721.
- 282 Azpiroz-Zabala, M., Cartigny, M.J.B., Talling, P.J., Parsons, D.R., Sumner, E.J., Clare, M.A., Simmons,
283 S.M., Cooper, C., and Pope, E.L., 2017b, Newly recognized turbidity current structure can explain
284 prolonged flushing of submarine canyons: *Science advances*, v. 3, p. e1700200,
285 doi:10.1126/sciadv.1700200.
- 286 Baas, J.H., Van Kesteren, W., and Postma, G., 2004, Deposits of depletive high-density turbidity currents:
287 a flume analogue of bed geometry, structure and texture: *Sedimentology*, v. 51, p. 1053–1088,
288 doi:10.1111/j.1365-3091.2004.00660.x.
- 289 Babonneau, N., Savoye, B., Cremer, M., and Bez, M., 2010, Sedimentary Architecture in Meanders of a
290 Submarine Channel: Detailed Study of the Present Congo Turbidite Channel (Zaiango Project):
291 *Journal of Sedimentary Research*, v. 80, p. 852–866, doi:10.2110/jsr.2010.078.
- 292 Bagnold, R.A., 1966, *An Approach to the Sediment Transport Problem from General Physics*: U.S.
293 Government Printing Office
- 294 Cantelli, A., Pirmez, C., Johnson, S., and Parker, G., 2011, Morphodynamic and Stratigraphic Evolution
295 of Self-Channelized Subaqueous Fans Emplaced by Turbidity Currents: *Journal of Sedimentary*
296 *Research*, v. 81, p. 233–247, doi:10.2110/jsr.2011.20.

- 297 Cartigny, M.J.B., Eggenhuisen, J.T., Hansen, E.W.M., and Postma, G., 2013, Concentration-dependent
298 flow stratification in experimental high-density turbidity currents and their relevance to turbidite
299 facies models: *Journal of Sedimentary Research*, v. 83, p. 1047–1065
- 300 Conway, K.W., Barrie, J.V., Picard, K., and Bornhold, B.D., 2012, Submarine channel evolution: active
301 channels in fjords, British Columbia, Canada: *Geo-Marine Letters*, v. 32, p. 301–312,
302 doi:10.1007/s00367-012-0280-4.
- 303 Edmonds, D.A., Shaw, J.B., and Mohrig, D., 2011, Topset-dominated deltas: A new model for river delta
304 stratigraphy: *Geology*.
- 305 Eggenhuisen, J.T., and McCaffrey, W.D., 2012, The vertical turbulence structure of experimental
306 turbidity currents encountering basal obstructions: implications for vertical suspended sediment
307 distribution in non-equilibrium currents: *Sedimentology*, v. 59, p. 1101–1120, doi:10.1111/j.1365-
308 3091.2011.01297.x.
- 309 Eggenhuisen, J.T., McCaffrey, W.D., Haughton, P.D.W., and Butler, R.W.H., 2010, Small-Scale Spatial
310 Variability in Turbidity-Current Flow Controlled by Roughness Resulting from Substrate Erosion:
311 Field Evidence for a Feedback Mechanism: *Journal of Sedimentary Research*, v. 80, p. 129–136,
312 doi:10.2110/jsr.2010.014.
- 313 Fernandes, A.M., Mohrig, D., and Buttles, J., 2018, A New Mechanism for Terrace Formation in
314 Submarine Canyons: *EarthArXiv*. September, v. 1, doi: 10.31223/osf.io/a6p7y
- 315 Garcia, M.H., 2008, *Sedimentation Engineering: Theories, Measurements, Modeling and Practice:*
316 *Processes, Management, Modeling, and Practice (Asce Manual and Reports on Engineering Practice*
317 *No: American Society of Civil Engineers.*
- 318 Garcia, M., and Parker, G., 1989, Experiments on hydraulic jumps in turbidity currents near a canyon-fan
319 transition: *Science*, v. 245, p. 393–396, doi:10.1126/science.245.4916.393.
- 320 Howard, A.D., 1994, A detachment-limited model of drainage basin evolution: *Water resources research*,
321 v. 30, p. 2261–2285, doi:10.1029/94WR00757.
- 322 Howard, A.D., 1980, Thresholds in river regimes: *Thresholds in geomorphology*, p. 227–258.
- 323 Hughes Clarke, J.E., 2016, First wide-angle view of channelized turbidity currents links migrating cyclic
324 steps to flow characteristics: *Nature communications*, v. 7, p. 11896, doi:10.1038/ncomms11896.
- 325 Janocko, M., Cartigny, M.B.J., Nemec, W., and Hansen, E.W.M., 2013, Turbidity current hydraulics and
326 sediment deposition in erodible sinuous channels: Laboratory experiments and numerical
327 simulations: *Marine and Petroleum Geology*, v. 41, p. 222–249,
328 doi:10.1016/j.marpetgeo.2012.08.012.
- 329 Johnson, J.P., and Whipple, K.X., 2007, Feedbacks between erosion and sediment transport in
330 experimental bedrock channels: *Earth Surface Processes and Landforms*, v. 32, p. 1048–1062,
331 doi:10.1002/esp.1471.
- 332 Johnson, J.P.L., Whipple, K.X., Sklar, L.S., and Hanks, T.C., 2009, Transport slopes, sediment cover, and
333 bedrock channel incision in the Henry Mountains, Utah: *Journal of geophysical research*, v. 114, p.
334 W12446, doi:10.1029/2007JF000862.
- 335 Kane, I.A., McCaffrey, W.D., and Peakall, J., 2008, Controls on sinuosity evolution within submarine

- 336 channels: *Geology*, v. 36, p. 287–290, doi:10.1130/G24588A.1.
- 337 Khripounoff, A., Vangriesheim, A., Babonneau, N., Crassous, P., Dennielou, B., and Savoye, B., 2003,
338 Direct observation of intense turbidity current activity in the Zaire submarine valley at 4000 m water
339 depth: *Marine geology*, v. 194, p. 151–158, doi:10.1016/S0025-3227(02)00677-1.
- 340 Leeder, M.R., and Bridges, P.H., 1975, Flow separation in meander bends: *Nature*, v. 253, p. 338,
341 doi:10.1038/253338a0.
- 342 de Leeuw, J., Eggenhuisen, J.T., and Cartigny, M.J.B., 2016, Morphodynamics of submarine channel
343 inception revealed by new experimental approach: *Nature communications*, v. 7, p. 10886,
344 doi:10.1038/ncomms10886.
- 345 Luthi, S. an, 1981, Experiments on non-channelized turbidity currents and their deposits: *Marine geology*,
346 v. 40, p. M59–M68, doi:10.1016/0025-3227(81)90139-0.
- 347 Métivier, F., Lajeunesse, E., and Cacas, M.-C., 2005, Submarine Canyons in the Bathtub: *Journal of*
348 *Sedimentary Research*, v. 75, p. 6–11, doi:10.2110/jsr.2005.002.
- 349 Middleton, G.V., 1966, Small-scale models of turbidity currents and the criterion for auto-suspension:
350 *Journal of Sedimentary Research*, v. 36, p. 202–208, doi:10.1306/74D71442-2B21-11D7-
351 8648000102C1865D.
- 352 Mitchell, N.C., 2014, Bedrock erosion by sedimentary flows in submarine canyons: *Geosphere*, v. 10, p.
353 892–904, doi:10.1130/GES01008.1.
- 354 Mohrig, D., and Buttles, J., 2007, Deep turbidity currents in shallow channels: *Geology*, v. 35, p. 155–
355 158, doi:10.1130/G22716A.1.
- 356 Nino, Y., Lopez, F., and Garcia, M., 2003, Threshold for particle entrainment into suspension:
357 *Sedimentology*, v. 50, p. 247–263, doi:10.1046/j.1365-3091.2003.00551.x.
- 358 Nittrouer, J.A., Mohrig, D., and Allison, M., 2011a, Punctuated sand transport in the lowermost
359 Mississippi River: *Journal of geophysical research*, v. 116, p. F04025, doi:10.1029/2011JF002026.
- 360 Nittrouer, J.A., Mohrig, D., Allison, M.A., and Peyret, A.-P.B., 2011b, The lowermost Mississippi River:
361 a mixed bedrock-alluvial channel: *Sedimentology*, v. 58, p. 1914–1934, doi:10.1111/j.1365-
362 3091.2011.01245.x.
- 363 Pirmez, C., Beaubouef, R.T., Friedmann, S.J., and Mohrig, D.C., 2000, Equilibrium profile and baselevel
364 in submarine channels: examples from Late Pleistocene systems and implications for the architecture
365 of deepwater reservoirs, *in* *Global deep-water reservoirs: Gulf Coast Section SEPM Foundation 20th*
366 *Annual Bob F. Perkins Research Conference*, p. 782–805.
- 367 Rowland, J.C., Hilley, G.E., and Fildani, A., 2010, A Test of Initiation of Submarine Leveed Channels by
368 Deposition Alone: *Journal of Sedimentary Research*, v. 80, p. 710–727, doi:10.2110/jsr.2010.067.
- 369 Shepherd, R.G., and Schumm, S.A., 1974, Experimental Study of River Incision: *GSA Bulletin*, v. 85, p.
370 257–268, doi:10.1130/0016-7606(1974)85<257:ESORI>2.0.CO;2.
- 371 Shields, A., 1936, Anwendung der Aehnlichkeitsmechanik und der Turbulenzforschung auf die
372 Geschiebebewegung: PhD Thesis Technical University Berlin.

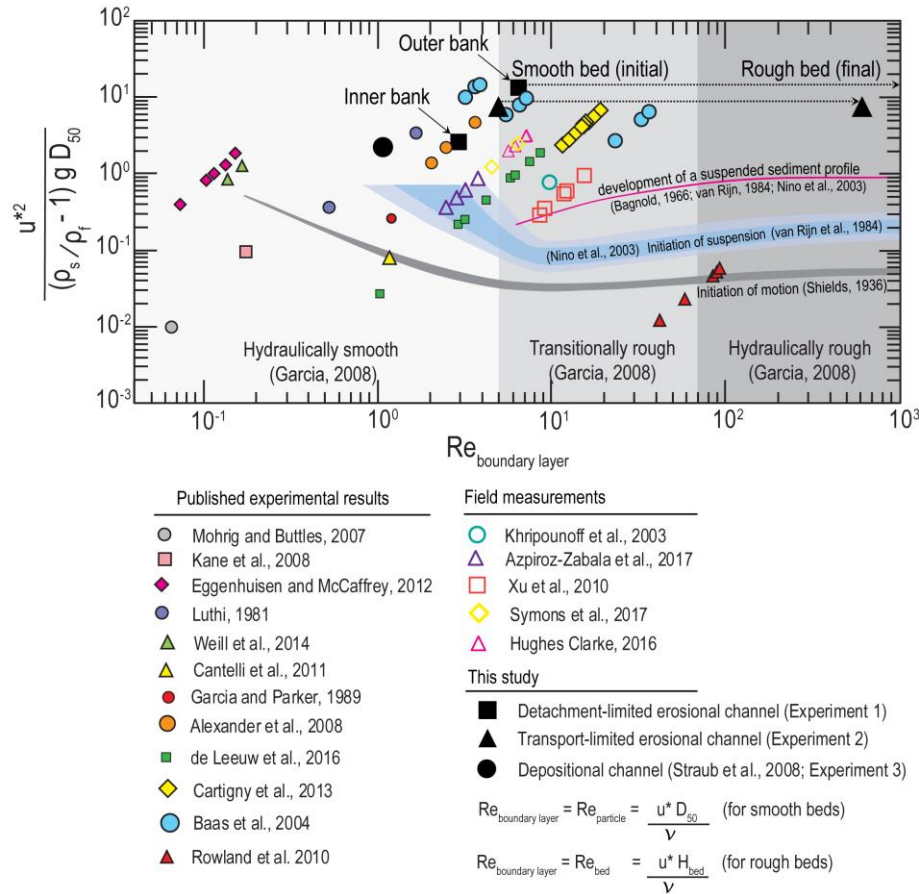
- 373 Sklar, L.S., and Dietrich, W.E., 2004, A mechanistic model for river incision into bedrock by saltating
374 bed load: *Water resources research*, v. 40, doi: 10.1029/2003WR002496.
- 375 Smith, J.D., and Hopkins, T.S., 1971, *Sediment Transport on the Continental Shelf Off of Washington*
376 *and Oregon in Light of Recent Current Measurements: Washington Univ., Seattle. Dept. of*
377 *Oceanography. Atomic Energy Commission, U. S. A.*
- 378 Straub, K.M., Mohrig, D., Buttles, J., McElroy, B., and Pirmez, C., 2011, Quantifying the influence of
379 channel sinuosity on the depositional mechanics of channelized turbidity currents: A laboratory
380 study: *Marine and Petroleum Geology*, v. 28, p. 744–760, doi:10.1016/j.marpetgeo.2010.05.014.
- 381 Straub, K.M., Mohrig, D., McElroy, B., and Buttles, J., 2008, Interactions between turbidity currents and
382 topography in aggrading sinuous submarine channels: A laboratory study: *GSA Bulletin today: a*
383 *publication of the Geological Society of America*, doi: 120/3-4/368/2260.
- 384 Symons, W.O., Sumner, E.J., Paull, C.K., Cartigny, M.J.B., Xu, J.P., Maier, K.L., Lorenson, T.D., and
385 Talling, P.J., 2017, A new model for turbidity current behavior based on integration of flow
386 monitoring and precision coring in a submarine canyon: *Geology*, v. 45, p. 367–370,
387 doi:10.1130/G38764.1.
- 388 Vachtman, D., Mitchell, N., and Gawthorpe, R., 2013, Morphologic signatures in submarine canyons and
389 gullies, central USA Atlantic continental margins: v. 41, p. 250–263,
390 doi:10.1016/j.marpetgeo.2012.02.005.
- 391 van Rijn Leo C., 1984, Sediment Transport, Part III: Bed forms and Alluvial Roughness: *Journal of*
392 *Hydraulic Engineering*, v. 110, p. 1733–1754, doi:10.1061/(ASCE)0733-9429(1984)110:12(1733).
- 393 Weill, P., Lajeunesse, E., Devauchelle, O., Métiver, F., Limare, A., Chauveau, B., and Mouazé, D., 2014,
394 Experimental investigation on self-channelized erosive gravity currents: *Journal of Sedimentary*
395 *Research*, v. 84, p. 487–498. Doi: 84/6/487/145405.
- 396 Whipple, K.X., 2004, Bedrock Rivers and the Geomorphology of Active Orogens: *Annual review of earth*
397 *and planetary sciences*, v. 32, p. 151–185, doi:10.1146/annurev.earth.32.101802.120356.
- 398 Whipple, K.X., Hancock, G.S., and Anderson, R.S., 2000, River incision into bedrock: Mechanics and
399 relative efficacy of plucking, abrasion, and cavitation: *GSA Bulletin*, v. 112, p. 490–503,
400 doi:10.1130/0016-7606(2000)112<490:RIIBMA>2.0.CO;2.
- 401 Xu, J.P., 2010, Normalized velocity profiles of field-measured turbidity currents: *Geology*, v. 38, p. 563–
402 566, doi:10.1130/G30582.1.
- 403 Xu, J.P., Barry, J.P., and Paull, C.K., 2013, Small-scale turbidity currents in a big submarine canyon:
404 *Geology*, v. 41, p. 143–146, doi:10.1130/G33727.1.
- 405 Xu, J.P., Noble, M.A., and Rosenfeld, L.K., 2004, In-situ measurements of velocity structure within
406 turbidity currents: *Geophysical research letters*, v. 31, doi:10.1029/2004GL019718.
- 407 Yu, B., Cantelli, A., Marr, J., Pirmez, C., O’Byrne, C., and Parker, G., 2006, Experiments on Self-
408 Channelized Subaqueous Fans Emplaced by Turbidity Currents and Dilute Mudflows: *Journal of*
409 *Sedimentary Research*, v. 76, p. 889–902, doi:10.2110/jsr.2006.069.

410

411 **Figures and captions:**

412

413



428

429 Figure 2: The modified Shield’s scaling approach of de Leeuw et al., 2016, used here to compare our
 430 experiments to various experimental and field studies. Note that the initial conditions in all 3 experiments
 431 presented in this study span the threshold between hydraulically smooth and transitionally rough flow.

432 Bed roughness that evolved in Experiments 1 and 2 increased the turbulence in the boundary, causing it to
 433 become hydraulically rough. (Luthi, 1981; Garcia and Parker, 1989; Khripounoff et al., 2003; Baas et al.,
 434 2004; Mohrig and Buttles, 2007; Alexander et al., 2007; Straub et al., 2008; Kane et al., 2008; Xu, 2010;
 435 Rowland et al., 2010; Cantelli et al., 2011; Eggenhuisen and McCaffrey, 2012; Cartigny et al., 2013;
 436 Weill et al., 2014; de Leeuw et al., 2016; Hughes Clarke, 2016; Symons et al., 2017; Azpiroz-Zabala et

437 al., 2017b). Hydraulic thresholds based on (Shields, 1936; Bagnold, 1966; van Rijn Leo C., 1984; Nino et
438 al., 2003; Garcia, 2008)

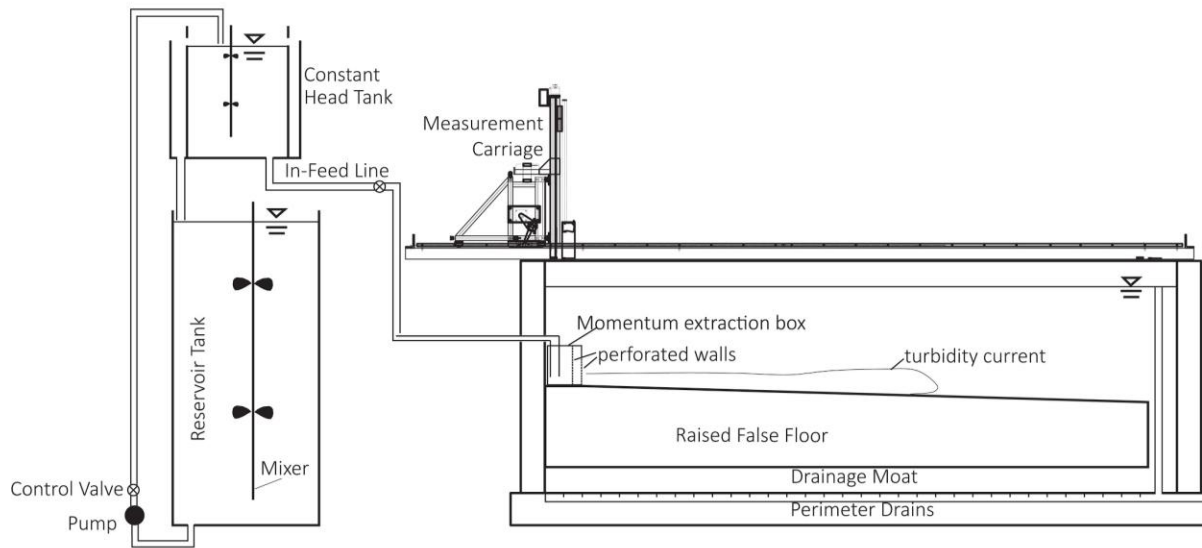


Figure 2: A generalized schematic of the experimental basin set-up used for the three experiments.

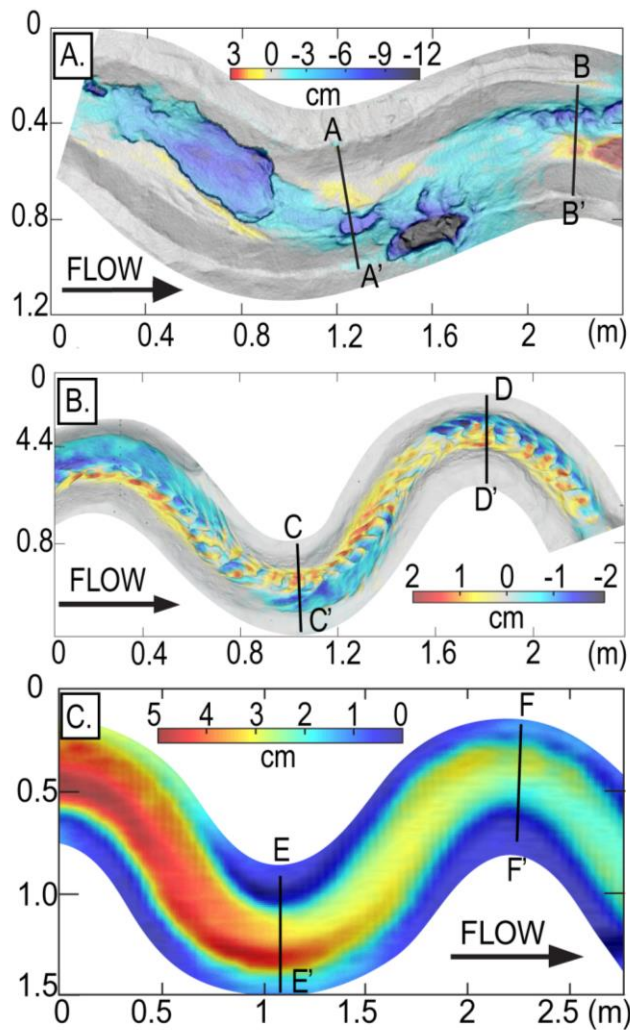


Figure 3: Difference maps defining net elevation change in all three experiments.. (A) Detachment-limited erosion in Experiment 1 resulted in a rough bed patterned with erosional bedforms along a semi-continuous erosional inner channel that followed the path of the high velocity core, and terraces formed at inner banks. (B) Transport-limited erosion in Experiment 2 resulted in a semi-continuous mobile sediment bed, reworked into ripples. (C) Consistent deposition in Experiment 3 resulted in a channel that was persistently aggradational, with the thickest deposits at the outsides of bends.

456

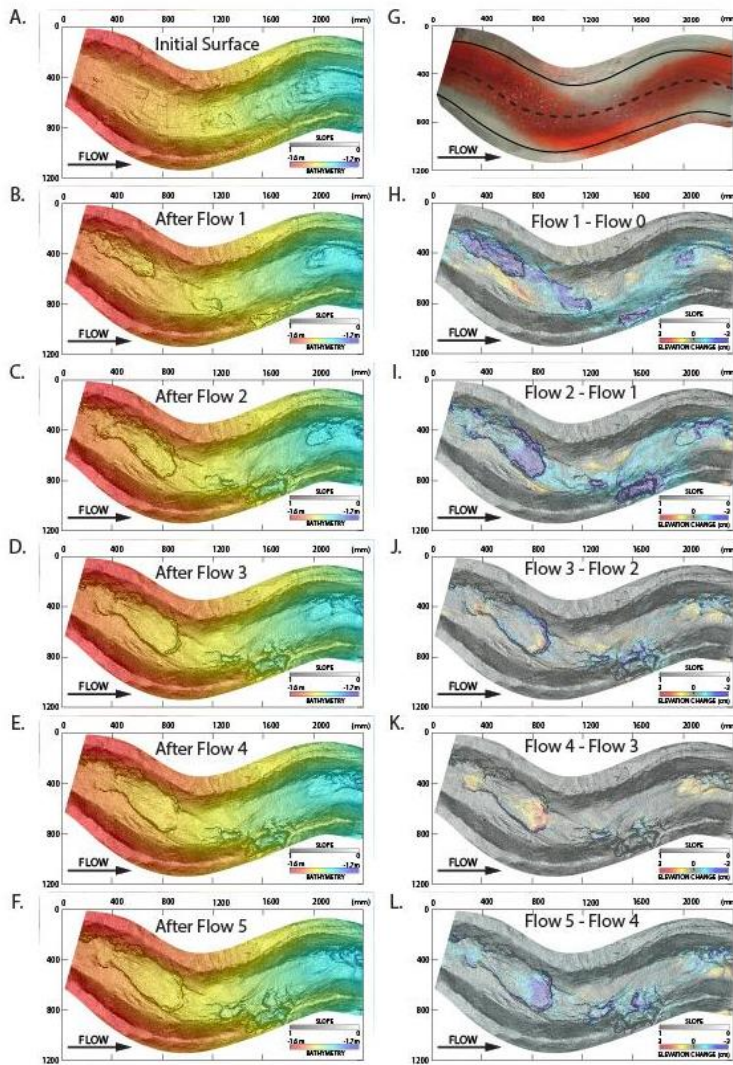


Figure 4: (A-F) Experiment 1 time-lapse laser-scanned topographic maps showing how the 5 experimental currents evolved the experimental channel. (G) Orthorectified overhead photograph showing the pathway of the high velocity core of the current-tracked by red dye with the most intensity. The very small amounts of red dye near the inner banks bear testament to very low velocities in these zones. (H-L) is a series of difference maps that define patterns of erosion and deposition within the experimental channel due to the passage of the 5 density currents. Note how erosion (cold colors) tracks the

474 pathway of the high velocity core (intense red dye in G) and no erosion weak deposition (warm colors) is
475 associated with inner bank zones visited by separated flow (low amount of red dye in G).

476

477

478

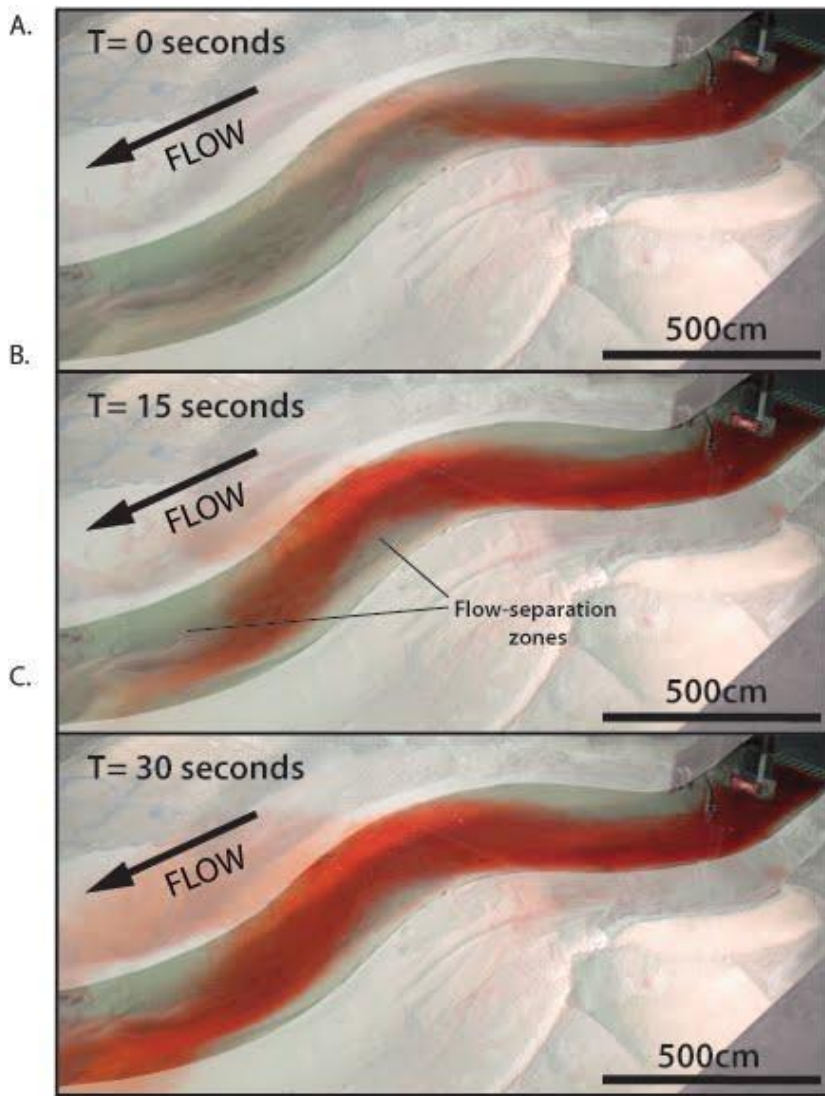
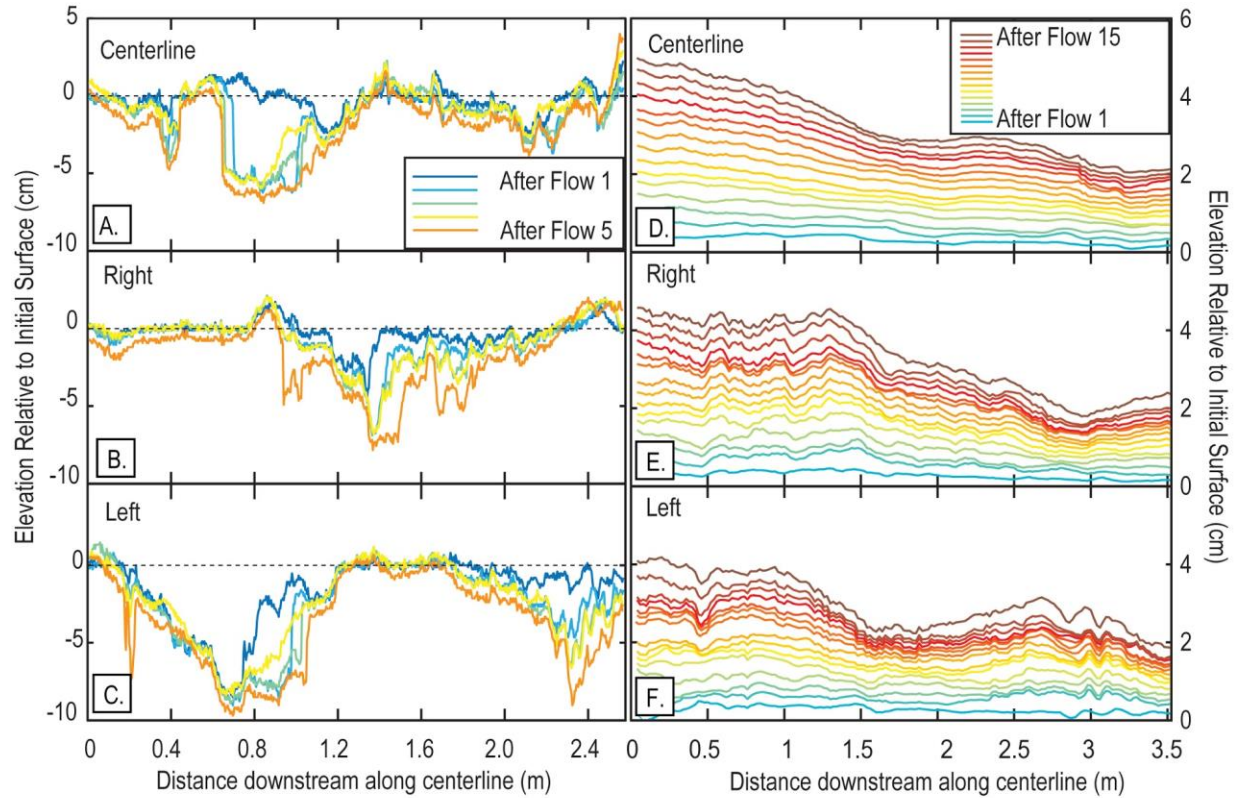


Figure 5: A-C Time lapse photographs showing a pulse of red dye in the current that defines the pathway of the high-velocity core of the current. Low velocity zones where flow separated from the inner banks received the dyed current later than the outside of bends and the dye intensity was always lower than at the outside of bends.

496

497

498



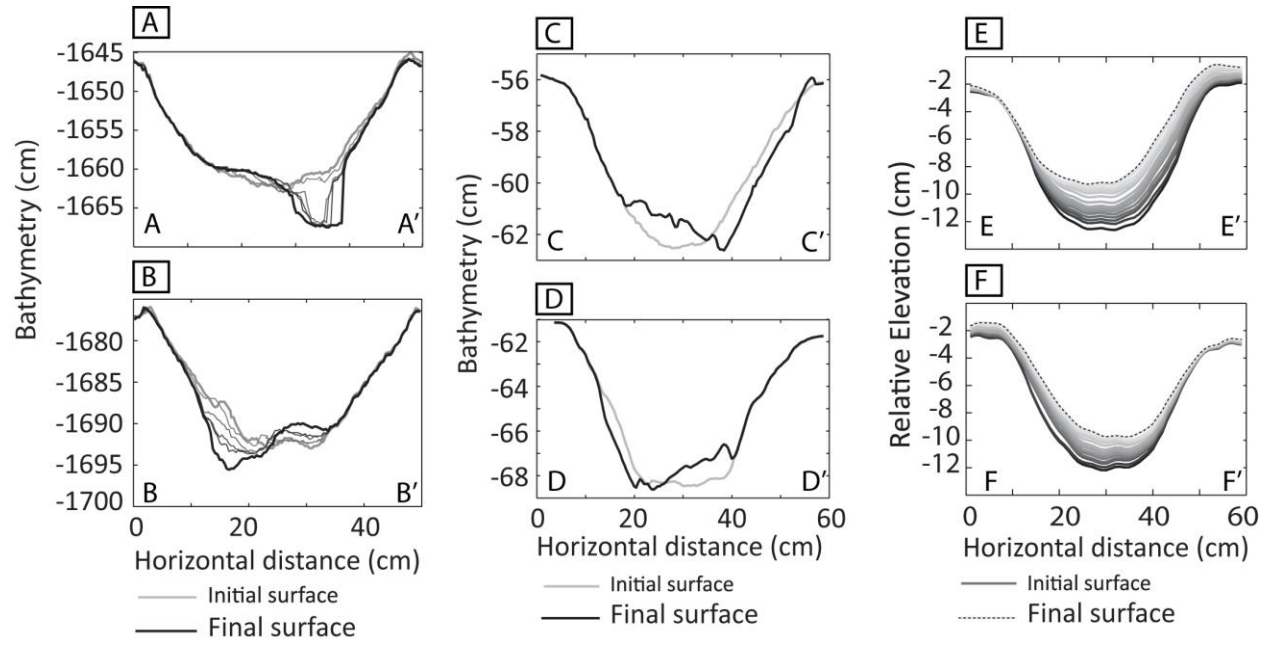
499

500 Figure 6: A-C) Change in elevation of the channel bed in Experiment 1 after the passage of 5 consecutive
501 flows, along (A) the centerline, (B) 15 cm right of the centerline, and (C) 15 cm left of the centerline. D-
502 F) Change in elevation of the channel bed in Experiment 3 after the passage of 15 consecutive flows,
503 along (A) the centerline, (B) 5 cm right of the centerline, and (C) 5 cm left of the centerline.

504

505

506



507

508 Figure 7: Cross sections showing time-lapse topographic evolution at the apices of the second and third
509 bends in Experiment 1 (A-B), Experiment 2 (C-D) and Experiment 3 (E-F).